



## Improving light output and coincidence time resolution of scintillating crystals using nanoimprinted photonic crystal slabs

Rosalinde Hendrika Pots<sup>a,b,\*</sup>, Matteo Salomoni<sup>a,c</sup>, Stefan Gundacker<sup>a,c</sup>, Silvia Zanettini<sup>d</sup>, Valentin Gâté<sup>d,e</sup>, Elise Usureau<sup>e</sup>, Daniel Turover<sup>d,e</sup>, Paul Lecoq<sup>a</sup>, Etienne Auffray<sup>a</sup>

<sup>a</sup> CERN, CH-1211, Geneva 23, Switzerland

<sup>b</sup> RWTH Aachen, Templergraben 55, 52062 Aachen, Germany

<sup>c</sup> Università degli studi di Milano Bicocca, Piazza dell'Ateneo Nuovo 1, 20126 Milano, Italy

<sup>d</sup> SILSEF SAS, 382 rue Louis Rustin, Archamps Technopole, F74160 Archamps, France

<sup>e</sup> NAPA Technologies SAS, 382 rue Louis Rustin, Archamps Technopole, F74160 Archamps, France

### ARTICLE INFO

#### Keywords:

Scintillators  
Photonic crystals  
Coincidence time resolution  
Light yield  
Nanoimprint lithography  
Fast timing detector

### ABSTRACT

Scintillating crystals are used in numerous applications of ionizing radiation detectors. In time of flight positron emission tomography (TOF-PET) for example, both energy and coincidence time resolution (CTR) are important characteristics that could significantly benefit if more light from scintillators, otherwise trapped, could be collected by the photodetector. A novel and promising method to extract more efficiently the light produced in crystal scintillators with high index of refraction is to introduce a thin nanopatterned photonic layer on the readout surface. In this paper, we describe the patterning process of a photonic crystal layer made of TiO<sub>2</sub> with 390 nm diameter "pillars" in a square lattice with a periodicity of 580 nm and a structure thickness of 300 nm on one side of a 10x10x10 mm<sup>3</sup> LYSO cube. The production process used was nanoimprint lithography. A substantial increase in light yield of ≥ 50% has been measured in good agreement with our simulations. An interesting result from these measurements is that the improvement in light output is independent of whether the crystal is read out from its photonic patterned side or from the one opposite to it. For all cases studied, the energy resolution improved by a factor of 1.1. On the other hand, the CTR, being very threshold dependent, is unlike the light yield not subject to a constant improvement. It turns out that, at low thresholds, the gain (improvement) in CTR is limited to 1.2, and then rapidly increases to a value of more than 2 at higher thresholds. This is mainly explained by an additionally induced light transfer time spread of the photonic pattern. Several configurations with and without Teflon wrapping were investigated.

### 1. Introduction

Scintillating crystals are widely used for the detection of ionizing particles in various applications, e.g. in high energy physics calorimetry, medical detectors, and homeland security.

An important characteristic of scintillators is their energy resolution. In positron emission tomography (PET) applications, where scintillators are used to detect two 511 keV gammas from electron-positron annihilation, the energy resolution enables to filter out scattered and other background events having energies other than the 511 keV photoelectric events. High energy resolution ( $E_{res}$ ) increases the signal to noise ratio and hence the detector sensitivity. The statistical contribution to the energy resolution  $E_{res}$  depends on the collected light in the following way:

$$E_{res} \propto \frac{1}{\sqrt{LY_{coll}}}$$

where  $LY_{coll}$  denotes the measured light yield.

Furthermore, for time-of-flight PET (TOF-PET) systems the coincidence time resolution (CTR) also plays an important role. High CTR is sought to reduce noise hits along the line of response and thereby further improve the signal to noise-ratio. Similar to energy resolution, the CTR depends on the measured light yield (LY):

$$CTR \propto \frac{1}{\sqrt{LY_{coll}}}$$

Therefore, both the energy resolution and the CTR can be improved if more light is collected by the photodetector. One suitable way in this direction, e.g., is to select specific scintillators with a high intrinsic light yield or to wrap the scintillator with reflectors or diffusing materials such as Vikuiti [1] or Teflon. Also using optical coupling between the scintillator and photodetector helps improving light collection significantly. Nonetheless, using as an example a  $2 \times 2 \times 20$  mm<sup>3</sup> LYSO crystal

\* Corresponding author at: CERN, CH-1211, Geneva 23, Switzerland.

E-mail address: [rosalinde.hendrika.pots@cern.ch](mailto:rosalinde.hendrika.pots@cern.ch) (R.H. Pots).

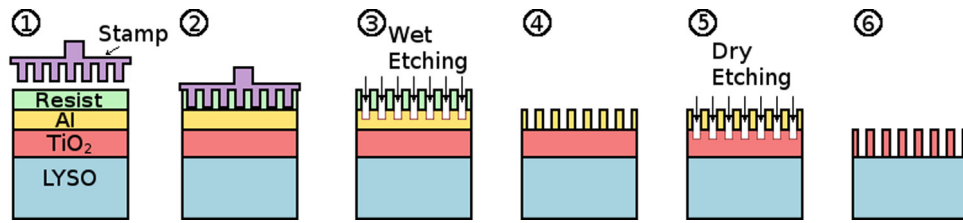


Fig. 1. Processing steps in nano-imprint lithography: (1) LYSO scintillator with subsequent layers of  $\text{TiO}_2$ , aluminum, and a resist deposited on its surface. (2) A stamp independently fabricated beforehand with the desired pattern imprints the pattern into the resist. (3) The pattern in the resist is transferred to the aluminum through wet-etching. (4) The imprinted aluminum layer has the pattern of the resist and is now used as a hard mask for the dry-etching process. (5) Dry-etching of the  $\text{TiO}_2$  transfers the Al-pattern to the  $\text{TiO}_2$ . (6) The hard mask is removed and the  $\text{TiO}_2$  is imprinted on the LYSO crystal with its final pattern.

wrapped with Teflon and mounted onto a PMT with optical coupling grease with index of refraction of 1.42 only 50% of the light produced in the crystal is extracted [2,3].

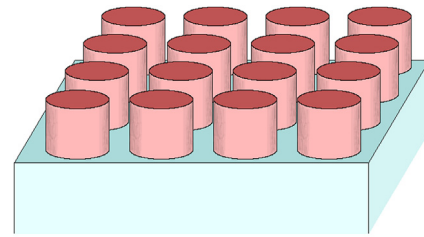
For specific applications, like PET and high energy calorimetry, scintillators are required to have high density so as to absorb a maximum of energy of the traversing ionizing particles. This generally results in a high refractive index ( $n = 1.82$  for LYSO) making light extraction from such scintillators difficult. If the medium, e.g. air, between the photodetector and the crystal has a lower refractive index, the interface between them will cause a significant amount of light to be trapped inside the crystal. Furthermore, the entry windows of photodetectors have a typical refractive index of the order of  $n = 1.5$ . This aggravates the mismatch in the involved indices even when applying an optical coupling between the scintillator and the photodetector. Therefore, there will always be a critical angle  $\theta_c$  that defines an extraction cone where every light outside of this cone will be internally reflected at the interface of the materials with different refractive indices.

A promising means to extract part of the (otherwise lost) light from outside of the extraction cone is to introduce a photonic crystal slab onto the readout surface of the scintillator. A photonic crystal slab is a thin layer of dielectric material imprinted on the scintillator with a periodic nanostructure where the periodicity is of the order of the wavelength of the light. If this structure is properly designed, it has the potential to significantly enhance light extraction through the diffraction of light impinging on the crystal's readout surface. In this way, light from higher than 0th order diffraction modes can be extracted beyond the extraction cone [4,5].

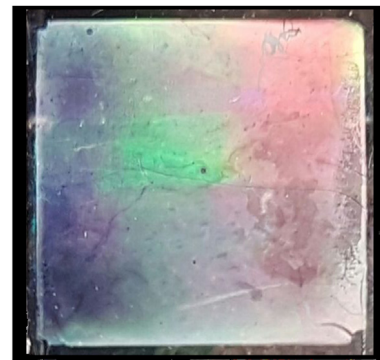
## 2. Produced sample

We have designed and produced a photonic crystal layer on the readout surface of a  $10 \times 10 \times 10 \text{ mm}^3$  LYSO:Ce cube to increase the amount of light to be extracted from this crystal. The cube used in this study was produced by Crystal Photonic, Inc. (CPI), with all six faces polished. On the bulk crystal, a  $\text{TiO}_2$  layer was imprinted with a nanopattern by SILSEF and NAPA Technologies [6], using nanoimprint lithography as shown in Fig. 1.  $\text{TiO}_2$  has a refractive index as high as 2.4 and is transparent to light emitted by LYSO:Ce at 420 nm. These are the two important features of any candidate material for photonic crystals [5]. The production method used for our slab is described in detail by the following six steps (see also Fig. 1:)

- First, a 300 nm layer of  $\text{TiO}_2$  is sputtered on one of the surfaces, usually denoted as the exit window of the crystal. Thereafter a layer of aluminum (Al) is deposited on the  $\text{TiO}_2$  coat, and then a resist applied on top of these (step 1 in Fig. 1).
- This is the layer onto which the desired pattern will then be imprinted via the nanoimprint lithographic process; it is a unique method where the pattern is imprinted into the resist layer with a so-called stamp (step 2 of Fig. 1) replicated from a master mold. The master mold itself is produced beforehand using electron beam lithography.



(a)



(b)

Fig. 2a-b. Illustrations of the photonic crystal pattern with pillars in a square lattice (a). Photo of the nanoimprinted surface of the LYSO:Ce cube showing the typical iridescent diffraction effects of photonic layers (b). Note, that the photonic pattern does not extend over the entire surface of the cube.

- After having imprinted the resist, the pattern is transferred to the aluminum layer via wet-etching (step 3) where the aluminum only serves as a hard mask for the dry-etching of the  $\text{TiO}_2$  (step 5), which will then produce the final, patterned layer on the scintillator (step 6). For our sample the chosen pattern consists of pillars arranged in a square lattice on top of the scintillator, as illustrated in Fig. 2a.

After the production of the photonic crystal on the bulk LYSO scintillator, the crystal is first visually inspected to assess how much of the surface is covered with the pattern, and to check for inhomogeneities visible by eye. Due to diffraction, the photonic crystal layer exhibits an iridescent shine on the scintillator surface, as seen in Fig. 2b.

To examine the fabricated pattern on the scintillator more closely, the photonic crystal slab was visualized with a scanning electron microscope (SEM). Since the sample is nonconductive and hence subject to electrostatic charging during the imaging process the resulting images are not perfectly sharp. By imaging the sample from the top, the periodicity and diameter of the pattern could be evaluated, but also possible defects in the shape of the structures and inhomogeneities in the pattern spotted. When the crystal is tilted one can also estimate the thickness of the nanostructure close to the edges of the crystal.

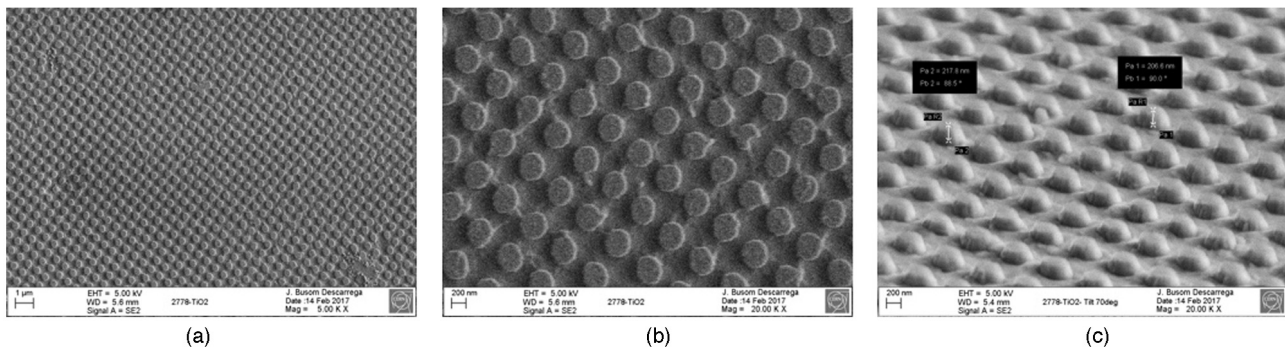


Fig. 3a-c. SEM images: made from top of sample with 4k magnification (a); top view SEM image with 20k magnification (b); SEM image of sample tilted by 70 degrees with 20k magnification (c).

Figs. 3a and 3b show SEM images recorded of the sample, all seen from top-down. The pattern shows regular periodicity and exhibits almost no defects. The diameter of the pillars on the pattern was measured to be 390 nm and the periodicity of the pattern to be 580 nm.

Fig. 3c gives an image of the sample when tilted by 70 degrees. After inspection of multiple images, we come to an average pillar height of 180 nm. Since the original  $\text{TiO}_2$  layer was 300 nm thick this would then give rise to the assumption that the  $\text{TiO}_2$  layer between the pillars was not entirely etched away, i.e. all the way down to the bare scintillator surface. This could have been caused by too short an exposure time during the etching process (step 4 in Fig. 1), therefore possibly leaving a residual  $\text{TiO}_2$  layer of  $\sim 120$  nm.

### 3. Simulations

#### 3.1. Simulation framework

A simulation framework was set up to predict the increase in the amount of light extracted from the scintillator with a photonic crystal slab on the scintillator's readout surface compared to a bare scintillator. This scheme consists of Geant4 simulating the macroscopic part of our system, and CAMFR modeling the nano-patterned photonic crystal slab. Geant4 is a free toolkit for the simulation of the passage of particles through matter [7]. CAMFR is a so-called "Maxwell solver", based on eigenmode expansion [5,8].

With Geant4 we simulate the light production in the LYSO cube due to radiation being converted inside the crystal and determine the trajectories of the produced scintillation photons in the cube, potentially including reflective wrapping. The LYSO cube is modeled with a surface roughness of  $\sigma_\alpha = 1.7^\circ$ , where the meaning of  $\sigma_\alpha$  is described in [9], except for the edges [3,10] simulated with a different  $\sigma_\alpha$  of  $57^\circ$ . From this Geant4 simulation we extract the angular distribution of the light impinging on the scintillator's readout surface from the *interior* of the crystal.

In CAMFR we define the shape of the photonic crystal. CAMFR then calculates the behavior of this pattern on the incident light using as input the internal angular light distribution produced before by Geant4 and, in this way, determines how much of the light is extracted and how much of it reflected. It is important to note that CAMFR is an analytical tool that simulates a pattern without defects. It is impossible to simulate the effect of non-periodic defects and therefore estimate their relevance.

#### 3.2. Results

We have simulated the pattern obtained from the SEM on our sample, in other words the pillars of 300 nm height and a diameter of 390 nm in a square lattice with 580 nm periodicity. The transmission of the 420 nm light in this photonic crystal slab is shown in Fig. 4.

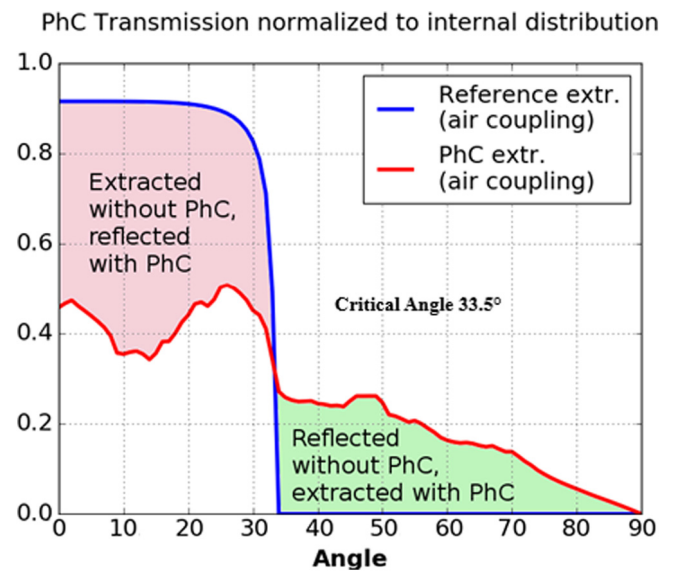


Fig. 4. Simulation of light transmission at the LYSO crystal–air interface, with and without a 300 nm thick photonic crystal layer as described above. The red-shaded area indicates light internally reflected by the photonic crystal, coming from the *inside* of the extraction cone that otherwise would have exited the crystal in the case of no photonic pattern. The green-shaded area indicates extracted light from *outside* of the extraction cone, i.e. light that would have been internally reflected and thus lost without the photonic nanopattern. (For interpretation of the references to color in this figure legend, the reader is referred to the web version of this article.)

The red-shaded area in the graph of Fig. 4 shows that the photonic nanopattern reflects a fraction of the light coming from the *inside* of the extraction cone that otherwise would have been extracted with no photonic pattern on the crystal. On the other hand, the green-shaded area in Fig. 4 denotes that part of the light that lies *outside* of the extraction cone, i.e. light that would have been reflected internally and hence lost without the photonic slab, and now being extracted because of this layer. Furthermore, light still not being extracted by the photonic crystal is understood to be internally reflected by the photonic crystal in a diffracted manner and therefore under angles different from the incident angle. As angles of the reflected light from outside of the extraction cone change, a significant fraction of this light is reflected inside the extraction cone and can therefore be extracted from the opposite side of the cube at the non-patterned crystal face. This provides an additional benefit in light yield when one reads out the crystal from the face opposite to the patterned surface.

Simulations were run for the following cases: a cubic  $10 \times 10 \times 10$  mm<sup>3</sup> LYSO crystal, coupled to air, with and without a photonic crystal slab, and also with and without Teflon wrapping as a comparison. Figs. 5a and 5b, respectively, show their effect on light extraction. In

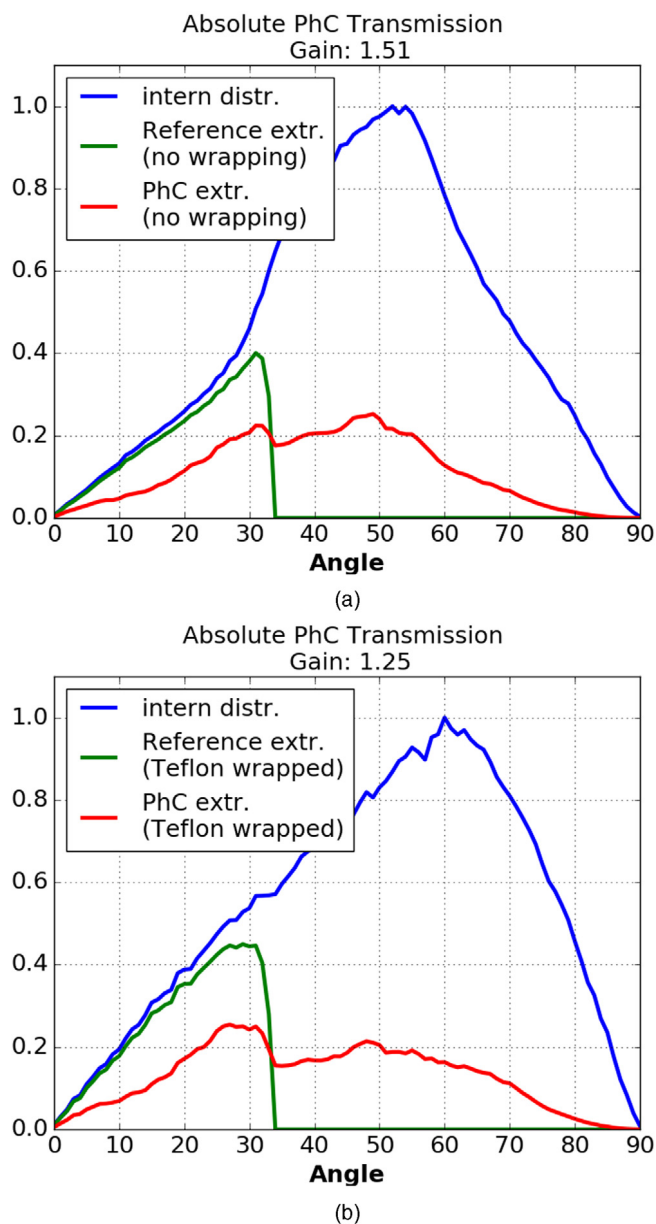


Fig. 5a-b. Simulation of light transmission at the crystal-air interface, in the case of a  $10 \times 10 \times 10 \text{ mm}^3$  LYSO cube equipped with and without a photonic layer for the two cases that the scintillator is unwrapped (left) and wrapped with Teflon (right). For both cases, the crystal is coupled via air at the photodetector interface.

Table 1

Simulated gain in light yield at first incidence for a  $10 \times 10 \times 10 \text{ mm}^3$  LYSO cube with a photonic crystal of 300 nm thickness minus a residual  $\text{TiO}_2$  layer, 390 nm in diameter and with a periodicity of 580 nm.

	Residual $\text{TiO}_2$ Layer [nm]	
	0	120
LY Gain without Teflon:	1.51	1.59
LY Gain with Teflon:	1.25	1.35

the case where there is no wrapping (Fig. 5a), we calculate a light gain of 1.51 due to the photonic crystal layer at first incidence. In the case, however, where the scintillator cube is wrapped with Teflon the benefit from the photonic layer is reduced resulting in a gain of only 1.25 at first incidence. This difference is attributed to the two different internal angular light distributions (due to different light reflection

from the side walls and the back of the crystal) from the two separate configurations studied.

Further simulations were made to understand the effect of a possible residual  $\text{TiO}_2$  layer estimated to be 120 nm thick, i.e. a remnant layer from a possibly incomplete etching process, as observed in the SEM image in Fig. 3c and discussed above. The effect of a residual  $\text{TiO}_2$  thickness of 120 nm was simulated and is shown in Table 1. In these simulations we have assumed the total thickness of the  $\text{TiO}_2$  layer prior to etching to be 300 nm. Absorption by the residual  $\text{TiO}_2$ , however, was not considered, since it is highly transparent to 420 nm light. Simulated gain in light yield at first incidence for a  $10 \times 10 \times 10 \text{ mm}^3$  LYSO cube with a photonic crystal of 300 nm thickness minus a residual  $\text{TiO}_2$  layer, 390 nm in diameter and with a periodicity of 580 nm.

From this we infer that the presence of the residual  $\text{TiO}_2$  layer does not necessarily lead to a degradation in light output; it may even have a beneficial effect on the light yield. Further studies are needed though to corroborate this assumption.

## 4. Measurements

### 4.1. Characterization methods

#### 4.1.1. Light yield

The light yield is measured by exciting the scintillating crystal with a  $^{137}\text{Cs}$  gamma source. The generated light is collected by a photomultiplier (Hamamatsu R2059) mounted, without optical coupling, to one face of the crystal. The PMT signal is digitized, and an energy spectrum produced. The position of the photopeak is then equivalent to the number of collected photons. The ratio between light measured with an un-patterned and patterned crystal defines the gain in light yield due to the introduced pattern.

#### 4.1.2. CTR

The test bench for the CTR measurements consists of two scintillators facing each other in a back-to-back arrangement and being excited by two correlated and colinear gammas (511 keV) from a  $^{22}\text{Na}$  source. As one of the crystals is used as a standard or reference crystal with its own intrinsic time resolution determined from an independent CTR measurement prior to our test series, the time resolution of the crystals under investigation can be derived from the deconvolution of the reference time resolution and the jointly measured CTR. Both the reference crystal and the crystal under test are coupled to a SiPM; in our case, the crystal under test is coupled to the SiPM with an air gap, from where the signal is split (a) for time stamping with a high frequency amplifier ( $\sim 1.5 \text{ GHz}$  bandwidth) [11] and (b) for an independent pulse height measurement with a low-noise analog operational amplifier [11], geared to obtain the energy of the photoelectric peak. The signals are digitized by a LeCroy DDA 735Zi oscilloscope. After event selection constraining data to the photopeak (511 keV events), the joint CTR is derived from the FWHM of the Gaussian fit of the correlated time stamp (time delay) histogram. In order to measure the light signal from the  $10 \times 10 \times 10 \text{ mm}^3$  LYSO:Ce cube, we used a Hamamatsu S13360 SiPM with

$6 \times 6 \text{ mm}^2$  size having  $50 \times 50 \mu\text{m}^2$  single photon avalanche diodes. This means that not the whole surface area was coupled to the SiPM and only the central light was measured, resulting in a deterioration of the CTR. Nevertheless, this does not compromise the validity of comparison studies.

### 4.2. Results from light yield and energy resolution measurements

LY was investigated and compared for two wrapping scenarios, i.e. without and with Teflon wrapping of the crystals, and respectively three and two configurations each:

#### 1. Without Teflon wrapping (three configurations)

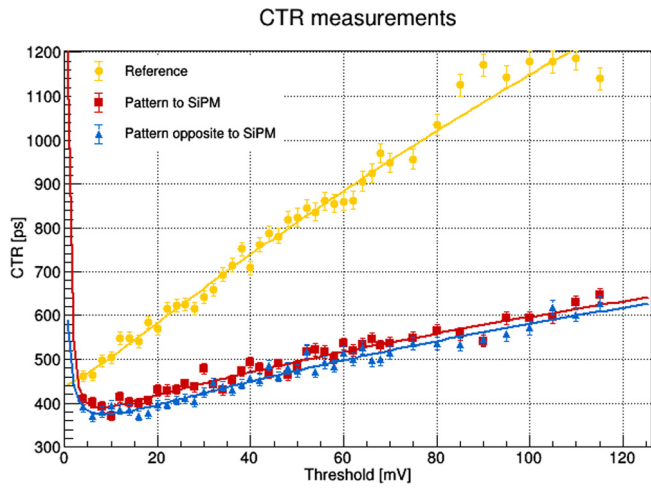


Fig. 6. Coincidence time resolution obtained from a nanoimprinted LYSO cube without Teflon wrapping or optical coupling mounted on a SiPM, compared to a reference or un-patterned crystal: two crystal orientations w.r.t. the SiPM window were used: patterned-face-to-SiPM (red squares), and opposite-face-to-SiPM (blue triangles). The CTR is measured with a 3% accuracy. Data for the reference crystal are shown as yellow dots. For all three configurations, the first data point at a threshold of 2 mV is in the electronic noise floor of the readout and thus leads to very high CTR values (not shown in the plot).

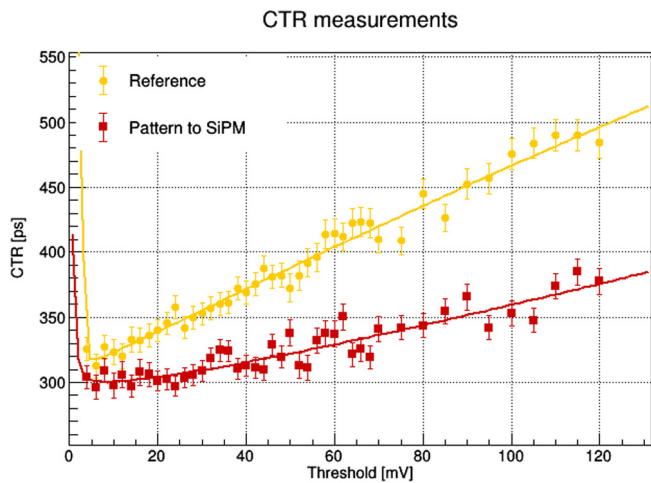


Fig. 7. Coincidence time resolution values of a nanoimprinted LYSO cube with Teflon wrapping (but no optical coupling) compared to a reference, un-patterned LYSO cube. The CTR is measured with a 3% accuracy. Measurements were made with a SiPM and high frequency readout. For both crystals, the first data point at a threshold of 2 mV is in the noise floor of the electronic readout.

- a. Non-patterned reference crystal mounted to PMT;
- b. Patterned crystal with patterned face mounted to PMT;
- c. Patterned crystal with opposite face mounted to PMT.

2. With Teflon wrapping (two configurations)

- a. Non-patterned reference crystal mounted to PMT;
- b. Patterned crystal with patterned face mounted to PMT.
- c. Measurements with the opposite face mounted to the SiPM were not performed in order not to damage the photonic pattern with the Teflon wrapping.

The results are shown in Table 2.

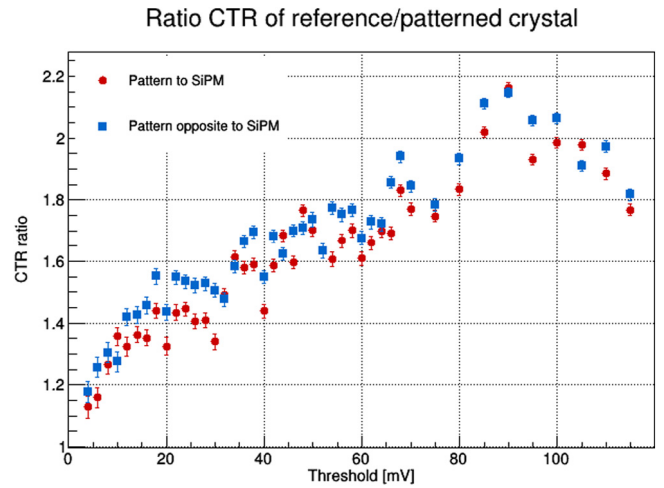


Fig. 8. Ratio of the CTRs obtained for the patterned and un-patterned crystal without Teflon wrapping at the same detector threshold. The CTR is measured with a 3% accuracy, leading to an accuracy of 4% for the measured ratio. This demonstrates that anywhere, other than near the noise threshold, the photonic crystal has superior performance, when it effectively improves CTR by more than a factor of two at highest thresholds.

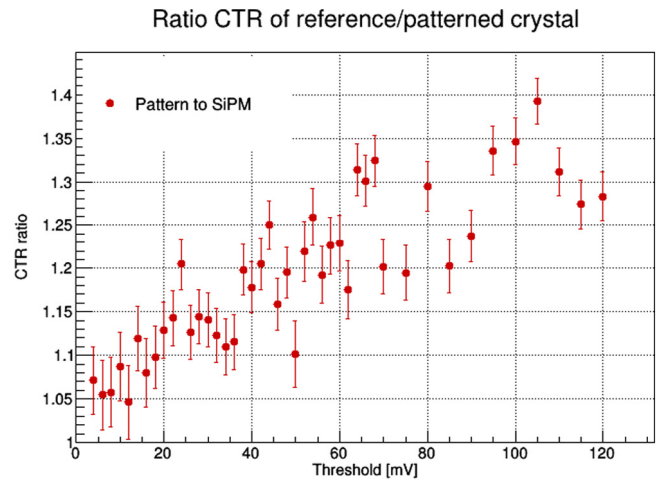


Fig. 9. Ratio of the CTRs obtained for the patterned crystal with Teflon-wrapping (in only one mounting position) and the reference crystal. The CTR is measured with a 3% accuracy, leading to an accuracy of 4% for the measured ratio. Data are taken without optical coupling at thresholds of  $\geq 2$  mV to avoid noise saturation.

4.2.1. PMT measurements without Teflon wrapping

For the case of no wrapping, the patterned crystal improves LY and energy resolution by a factor of 1.5 and 1.1 respectively. This is in good agreement with the simulations assuming 0 nm residual TiO<sub>2</sub> layer. It is interesting to see that a nearly identical gain in light yield is achieved when the crystal is read out from the untreated side, opposite to the patterned surface. This indeed is also expected from the simulations as explained in Section 3.2. The gain in energy resolution is in line with what one would expect on purely statistical grounds Eq. (1), taking into account the error on the measurement.

4.2.2. PMT measurements with Teflon wrapping

When the crystals, reference and patterned ones, are wrapped in Teflon, the relative gain in light yield drops to 1.4. This is slightly higher than expected from the simulations and could be an indication of the presence of the residual TiO<sub>2</sub> layer presumed in one of our simulation schemes, in which case the light yield would match the simulations perfectly. However, if the residual layer of 120 nm indeed

**Table 2**

Comparison of simulated and measured LY and energy resolution and their improvements (gain). Both LY and energy are measured with a 5% accuracy, leading to an accuracy of 7% for the measured gain.

	Simulated Gain with 0 nm residual TiO <sub>2</sub>	Simulated Gain with 120 nm residual TiO <sub>2</sub>	Measured LY with PMT [Ph/MeV] ( $\times 10^3$ )	Measured Energy-Resolution with PMT [%]	Measured Gain in LY with PMT	Measured Gain in Energy Resolution with PMT	Expected Gain in Energy Resolution from LY
Reference crystal without wrapping	–	–	4.4	19	–	–	–
PhC facing detector without wrapping	1.5	1.6	6.5	16	1.5	1.1	1.2
PhC from opposite side without wrapping	–	–	6.5	17	1.5	1.1	1.2
Reference crystal with wrapping	–	–	13	11	–	–	–
PhC facing detector with wrapping	1.3	1.4	19	9.4	1.4	1.2	1.2

exists, the crystal measurements without wrapping should also match the corresponding simulations, which is not the case. Another contribution to the slightly higher measured values with Teflon wrapping could be due to a difference in how the Teflon affects the directionality of the light in the simulations compared to the actual behavior. The energy resolution improves in a configuration with Teflon wrapping i.e. by a factor of 1.2, in line with photostatistics.

Comparison of simulated and measured LY and energy resolution and their improvements (gain). Both LY and energy are measured with a 5% accuracy, leading to an accuracy of 7% for the measured gain.

#### 4.3. Results from coincidence time resolution (CTR) measurements

Similar to our foregoing LY measurements, the CTR was investigated and compared for five different configurations as described in Section 4.2, however, using SiPMs instead of PMTs.

Over a large threshold range, i.e. 2–115 mV, and the above configurations a series of coincidence time resolution (CTR) measurements was made using the high frequency readout for time stamping as explained in Section 4.1.2. The results of these runs are shown in Fig. 6 (scenario 1) and Fig. 7 (scenario 2), where the CTR is plotted against the applied threshold.

From Fig. 6 (unwrapped scenario) we notice that the highest coincidence time resolution (i.e. lowest CTR value) is obtained for the photonic crystals of 390 ps FWHM with the patterned surface read out by the SiPM, and 375 ps when read out from the opposite crystal face (values taken from the fits in Fig. 6). In this scenario, the reference crystal achieves a CTR of 450 ps FWHM only. This translates into a CTR-gain of 1.2 at lowest thresholds increasing systematically towards higher threshold values (see also Fig. 8).

On the other hand, Fig. 7 (wrapped scenario) clearly shows that wrapped scintillators, as expected [12], provide higher time resolution than non-wrapped crystals. Yet, the photonic crystal still has a superior CTR than its reference counterpart, i.e. achieving 300 ps FWHM versus 317 ps FWHM (values taken from the fits in Fig. 7) constituting a factor of about 1.1 improvement as compared to the non-patterned crystal at low thresholds, and increasing steadily at higher thresholds (Fig. 9).

The measurements above also show that the CTR is very sensitive to threshold changes, though less pronounced for the photonic crystals compared to their untreated references. The same holds for those scintillators that are wrapped in Teflon in contrast to the unwrapped ones. This correlation is better visualized in Figs. 8 and 9 corresponding to unwrapped and wrapped crystals, respectively, where the CTR ratio of reference and photonic crystals is shown as a function of threshold.

In Tables 3 and 4, corresponding to the two scenarios of unwrapped and wrapped scintillators, we list some specific values for the gain in CTR at given thresholds and compare this with the CTR gain to be expected from LY measurements considering photostatistics only, i.e. taking the square root of the light yield gain. It can be seen that the resulting CTR improvements (gain) correlate (within the statistical

uncertainties) with the light yield gain for low thresholds, i.e.  $\sim 1.22$  ( $=\sqrt{1.5}$ ) versus a LY gain of 1.5 in the un-wrapped case. On the other hand, for the wrapped case, the expectation in CTR improvement considering pure photostatistics is higher, i.e.  $\sqrt{1.4} = 1.18$  as compared to the measured value of about 1.1.

The results demonstrate that the nanoimprinted scintillator transfers light more efficiently than an un-treated crystal. Additionally, and in line with our findings for LY and energy resolution, it again makes no difference from which side, front face or reversed, the crystal is read out.

The improvement in CTR over that of the reference device becomes rather high when raising thresholds to  $>10$  mV, notwithstanding its excellent values also at lower thresholds. It is also worth noting that the CTR of the patterned crystal is much less sensitive to threshold changes than the reference crystal. This is important for highly integrated systems, where tradeoffs in the electronic bandwidth and power consumption do not allow to operate the detectors at lowest thresholds possible.

The high dependence of the CTR gain on the leading-edge threshold, i.e. low gain for low thresholds and high gain for high thresholds, can be explained by the change of light transfer modes in the photonic crystal in contrast to its non-patterned counterpart. In order to investigate this behavior, we conducted very preliminary Monte-Carlo simulations and found that, if an additional photon transfer time spread due to the presence of the photonic layer is included, the modeled CTR improvement versus the leading-edge detection threshold approaches that of the measurements. The additional time smearing in the photonic crystal arises from the fact that about 50% of the direct photons are reflected back into the crystal whereas delayed photons that normally are not collected by the photodetector can now, under the influence of the nanopattern, reach the SiPM. This behavior can be understood by looking at Fig. 4, where larger angles for photons exiting the crystal also mean a longer travel path and therefore a larger delay time. Additional photons extracted by the photonic crystal at larger angles thus come at later times and do contribute to the signal formation at higher leading-edge thresholds and therefore improve the CTR at higher thresholds. On the other hand, the slightly reduced number of photons arriving very early at the photodetector lowers the CTR gain at lower thresholds.

In other words, the photonic pattern in this particular case transfers early arriving photons to later times, nevertheless, increasing the total amount of photons extracted. Hence, also at earlier times the number of photons is higher than in the non-patterned crystal and therefore improves the photostatistics leading to an overall improved CTR. In this sense the photonic pattern changes the weight of the diffractive modes. Depending on the application and the scintillator geometry this behavior varies, and it is even thinkable to use this feature of photonic crystals to optimize the time structure of detected photons in special cases.

**Table 3**

List of CTR measurements and their gain compared to expected values derived from LY measurements: All measurements are made without Teflon wrapping. The values are taken from the fits in Fig. 6. The CTR is measured with a 3% accuracy, leading to an accuracy of 4% for the measured gain in CTR. Considering the error in the measured gain in LY, the expected gain in CTR from the measured LY as an accuracy of about 4%.

Crystal face being read out:	Best measured CTR FWHM [ps]	CTR Improvement (Gain)			Expected from LY measured w/ PMT
		@ best CTR	@ 10 mV Threshold	@ 100 mV Threshold	
Reference crystal	450	–	–	–	–
Photonic	390	1.2	1.3	1.9	1.22
Opposite	375	1.2	1.3	2.0	1.22

**Table 4**

List of CTR measurements and their gain compared to expected values derived from LY measurements: All measurements are made with Teflon wrapping. The values are taken from the fits in Fig. 7. The CTR is measured with a 3% accuracy, leading to an accuracy of 4% for the measured gain in CTR. Considering the error in the measured gain in LY, the expected gain in CTR from the measured LY as an accuracy of about 4%.

Crystal face being read out:	Best measured CTR FWHM [ps]	CTR Improvement (Gain)			Expected from LY measured w/ PMT
		@ best CTR	@ 10 mV Threshold	@ 100 mV Threshold	
Reference crystal	317	–	–	–	–
Photonic	300	1.1	1.1	1.3	1.18

## 5. Summary and discussion

We have successfully produced a photonic crystal slab, manufactured via nanoimprint lithography and made of  $\text{TiO}_2$  on top of a  $10 \times 10 \times 10 \text{ mm}^3$  LYSO:Ce cube. The produced pattern is of high quality, where the imprinted structures have the desired shape of pillars with fine-grained periodicity. We have simulated the produced pattern and also the effect of a possible residual  $\text{TiO}_2$  layer left over from the etching process. From these simulations we can conclude that the residual layer does not necessarily have a detrimental effect and hence decrease the gain in light yield.

The photonic crystal delivers a significant increase in light yield, both when extracted from the patterned surface or from the face opposite to it. In the case that no wrapping of the crystal is used, the total gain in light yield is 1.5 and the corresponding improvement in energy resolution 1.1, irrespective of the two adjacent exit faces, patterned or un-patterned, being read out. This gain in light yield agrees with our predictions from the simulations. The gain in energy resolution, however, is slightly lower than expected from the equivalent gain in LY on arguments that only photostatistics is taken into account. This might be due to inhomogeneities in the nanopattern of the photonic crystal.

Time resolution seems to particularly benefit from photonic patterning, especially for bare (un-wrapped) crystals and at higher detection thresholds. In that case, gains in CTR ranging from 1.2 at low threshold to more than a factor of 2 at higher thresholds have been observed. Particularly, CTR improvements at highest time resolutions obtained near the detection threshold are well in line with our expectations from photostatistics and confirmed by the corresponding LY measurements. Still further work is needed to identify and factorize all influences, other than statistical ones, on the time resolution, especially for data at higher thresholds.

In the case where the tested crystals are wrapped in Teflon tape, a method traditionally used to increase their light yield, the “photonic” effect and its benefit on the time resolution become less pronounced than observed with bare crystals. In terms of LY and energy resolution we have observed an improvement of 1.4 and 1.1, respectively, owing to the photonic pattern, where the gain in energy resolution is slightly lower than expected from pure photostatistics. The obtained gains in CTR are, as we had expected from our simulations, more moderate accordingly, i.e. 1.1 at lowest threshold and 1.3 at higher thresholds.

In conclusion, it is shown that photonic imprinting of scintillators, in particular with the chosen process and its resulting high-quality

pattern, can significantly improve light yield, energy and time resolution in scintillator-based detection systems. While the effect is still modest as long as wrapped scintillators are used in conjunction with detectors operating at very low detection thresholds, the potential of this technique is far from being exhausted, hence giving new incentives for further investigations on the basis of novel and more elaborate patterns and their production methods. Those efforts could then include a comparison with different crystal surface states, such as de-polishing or micro-structuring of the crystal face. There is still room for improvement and optimization of suitable pattern types and shapes, in conjunction with different types of wrapping and optical coupling for the crystals.

## Acknowledgments

This research has been carried out in the framework of the Crystal Clear Collaboration. This work was supported by the Eurostars Eureka project No. 8974 (TURBOPET), ERC Advanced Grant No. 338953 (TICAL), ERC Proof of Concept Grant No. 680552 (Ultima), the Wolfgang Gentner Program of the German Federal Ministry of Education (grant No. 05E15CHA), CERN Knowledge Transfer Fund and collaboration CERN-Haute Savoie.

The authors are grateful to Thomas Meyer for his profound assistance and help in writing and editing this article.

## References

- [1] 3M, Vikuiti Enhanced Specular Reflector (ESR). Available at: [https://www.3m.com/3M/en\\_US/company-us/all-3m-products/~/~3M-Enhanced-Specular-Reflector-3M-ESR-/?N=5002385+3293061534&rt=rud](https://www.3m.com/3M/en_US/company-us/all-3m-products/~/~3M-Enhanced-Specular-Reflector-3M-ESR-/?N=5002385+3293061534&rt=rud).
- [2] S. Gundacker, F. Acerbi, E. Auffray, A. Ferri, A. Gola, M.V. Nemalappudi, G. Paternoster, C. Piemonte, P. Lecoq, State of the art timing in TOF-PET detectors with LUAG, GAGG and L(Y)SO scintillators of various sizes coupled to FBK-SiPMs, *J. Instrum.* 11 (08) (2016) P08008.
- [3] R. Martinez Turtos, S. Gundacker, M. Pizzichemi, A. Ghezzi, K. Pauwels, E. Auffray, P. Lecoq, M. Paganoni, Measurement of LYSO intrinsic light yield using electron excitation, *IEEE Trans. Nucl. Sci.* 63 (2) (2016) 475–479.
- [4] A. Knapitsch, P. Lecoq, Review on photonic crystal coatings for scintillators, *Internat. J. Modern Phys. A* 29 (30) (2014) 1430070.
- [5] Matteo Salomoni, Rosalinde Pots, Etienne Auffray, Paul Lecoq, Enhancing light extraction of inorganic scintillators using photonic crystals, *Crystals* 8 (2) (2018).
- [6] SILSEF SAS. Available at: <https://www.silsef.com>.
- [7] J. Allison, et al., Recent developments in geant4, *Nucl. Instrum. Methods Phys. Res. A* 835 (2016) 186–225.
- [8] CAMFR simulation tool. Available at: <http://camfr.sourceforge.net/>.

- [9] M. Janecek, W.W. Moses, Simulating scintillator light collection using measured optical reflectance, *IEEE Trans. Nucl. Sci.* 57 (3) (2010) 964–970.
- [10] K. Pauwels, E. Auffray, S. Gundacker, A. Knapitsch, P. Lecoq, Effect of aspect ratio on the light output of scintillators, *IEEE Trans. Nucl. Sci.* 59 (5) (2012) 2340–2345.
- [11] S. Gundacker, R. Martinez Turtos, E. Auffray, M. Paganoni, P. Lecoq, High-frequency sipm readout advances measured coincidence time resolution limits in TOF-PET, *Phys. Med. Biol.* 64 (2019) 055012, 9pp.
- [12] S. Gundacker, E. Auffray, K. Pauwels, P. Lecoq, Measurement of intrinsic rise times for various L(Y)SO and LuAG scintillators with a general study of prompt photons to achieve 10 ps in TOF-PET, *Phys. Med. Biol.* 61 (2016) 2802–2837.